ORIGINAL ARTICLE

G. La Valle · F. Fabbrocino · B. Desmorat

On the influence of microproperties of elastoplastic hinges on the global behavior of pantographic sheets in bias extensional test

Abstract Experimental observations have revealed a change in the concavity of the resultant force-displacement plot in the extension test for pantographic sheets. In this paper, we aim to relate these macroscopically observed mechanical properties with the microscale properties of the hinges (or pivots) connecting the pantographic fibers. The material constituting the hinges is modeled at the microscale as an isotropic elastoplastic 3D Cauchy continuum. The elastic regime is assumed to be linear, while the plastic regime exhibits either saturating or non-saturating hardening. In the case of circular homogeneous cylindrical hinges, monotonic loading is considered to derive a mesoscale constitutive relation linking the torsional angle to the total applied torque. It is demonstrated that (non-)saturating hardening at the microscale results in (non-)saturating hardening of the twist angle/torque plot at the mesoscale, which itself is responsible for the change of concavity in bias extensional test of pantographic sheets.

1 Introduction

In the theory of meta materials one of the most interesting problems concerns the synthesis of microstructures which at macro level have a certain well specified behavior [1–4]. This behavior is made precise by the choice of an action functional and a dissipation functional [5–8]. In [9,10], it is proven that an essential property of micro structures synthesizing second gradient continua consists in including elastic hinges and perfect pivots interconnecting bending fibres. Therefore, the technological problem of finding a 3D printing process producing perfect pivots and elastic hinges became relevant [11–14]. This problem seems to have found some usefully solutions [15,16]: however, a deeper theoretical insight is necessary in order to give the demanded support to such a complex technological demand. In the present paper, we start the modeling analysis necessary to fully understand the already available experimental evidences [9,10,12,17–21]. This knowledge will be useful in pursuing the important further step aiming to improve elastic range of hinges introduced in pantographic structures [22].

Albeit one could believe that non-linear elastic phenomena occur in bias extension test of pantographic sheets, here we prove that also plasticity at micro level does justify observed experimental evidences. The

G. La Valle
MSME UMR 8208, Université Gustave Eiffel, 5 bd Descartes, Marne-la-Vallée 77454, France
e-mail: gabrielelavalle@gmail.com

F. Fabbrocino
Dipartimento di Ingegneria, Centro Direzionale Isola F2, Università Digitale Pegaso, Naples, Italy

B. Desmorat (✉)
CNRS, UMR 7190, Institut Jean Le Rond d'Alembert, Sorbonne Université, 4 Place Jussieu, 75252 Paris, France
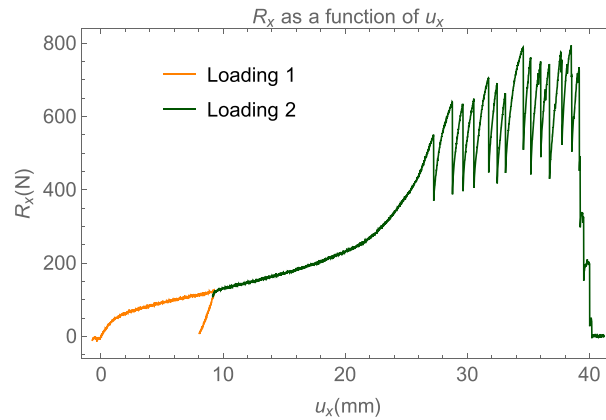e-mail: boris.desmorat@sorbonne-universite.fr

Fig. 1 $u_x \mapsto R_x$ experimental curve of a metallic pantographic sample in bias elongation test, where u_x denotes the horizontal displacement and R_x the corresponding reaction force

here postulated assumption is that elastic hinges reach, in some of their parts, plastic regime and therefore that macroscopically observed non linearity finds its fundamental description in an elastoplastic model for the material constituting the hinges. This is consistent with the specific materials used, up to now, to build using 3D printing techniques pantographic sheets. Of course, non linear elastic effects may need to be included in the modeling when building specimens with other materials.

The major novelty in the present paper is that we demonstrate by a closed form analysis across micro and mesoscale that the change of concavity observed in bias extensional test of pantographic sheets is explained by elasto-plasticity in the hinges of such pantographic sheets.

Moreover, our analysis allows for the determination of the class of materials using which pantographic microstructures produce macro second gradient materials [23–26] with largest elastic regime: in the conclusions we present a comparison among different materials in this respect and we give a qualitative rational explanation of the high performances of the polyamid when compared to iron, aluminium and nickel.

2 Experimental evidences and constitutive meso modelling difficulties

Advancements in additive manufacturing and 3D printing techniques have enabled the production of pantographic metamaterials with exceptionally fine microstructures [9,10,27,28]. For experimental evidence related to polyamide (PA) and metallic (ME) pantographic sheets subjected to bias extensional test, we refer to [29,30].

These experimental results are used to calibrate a multi-scale model, introducing three distinct scales: macroscopic, mesoscopic, and microscopic.

On the macroscale, the pantographic sheet subjected to a bias extension test results in a macroscopic force-displacement relationship. In the particular case of a ME pantographic sheet [30], the length scale of the macroscopic scale is characterized by the dimensions of the specimen which is 21 cm long and 7 cm wide. The macroscopic force-displacement relationship is presented in Fig. 1. This curve shows a change in concavity that is not observed in PA samples [29].

On the mesoscale, there are two main possible choices regarding the mesomodeling for describing the behavior of such a medium: continuous or discrete. If a continuous mesomodeling is chosen, a second-gradient continuum is typically used [31]. However, in this work, we will use a discrete meso-modeling approach. Specifically, we will employ the Hencky-type discrete model [12,32–34]. Here, the pantographic material is modeled as an assembly of extensional springs interconnected by rotational springs. Extensional springs account for the elongation of pantographic fibers, while rotational springs account for both fiber bending (see Fig. 2b) and torsion of interconnecting hinges (see Fig. 2c). The length scale of the mesoscopic scale is related to the order of magnitude of the size of the structural elements from which the pantographic sheet is made of (namely the length and diameter of hinges and the dimensions of the cross section of the fibers which are approximately equal to 5 mm in the pantographic sheets presented in this paper).

On the mesoscale, the constitutive law describing the torsional behavior of the interconnecting hinges is the function $\alpha \mapsto M(\alpha)$, where α is the twist angle of each hinge and M is the torsional moment. The strain energy is expressed as the sum of stretching, bending, and shear contributions [12]. The axial, bending, and
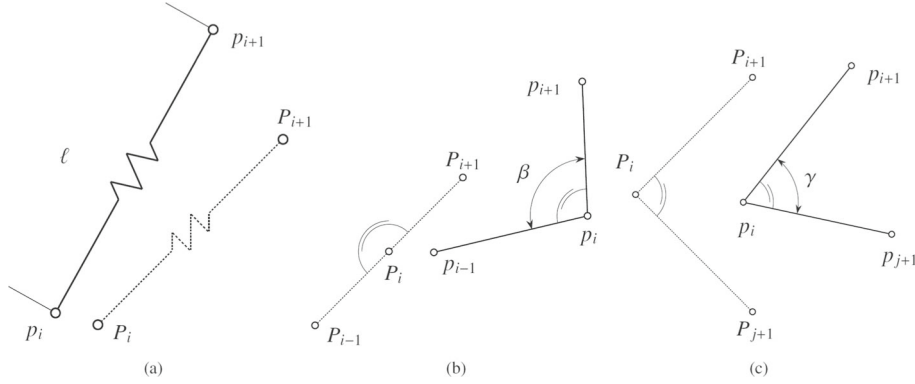
Fig. 2 Hencky-type model with: **a** axial extensional springs, **b** bending rotational springs and **c** torsional rotational springs

torsional specific energies, denoted as $\ell \mapsto w_a(\ell)$, $\beta \mapsto w_b(\beta)$, and $\alpha \mapsto w_s(\alpha)$, respectively, can be defined by equations [22]:

$$w_a(\ell) = \frac{1}{2}k_a \left(\ell - \ell_0\right)^2 \qquad w_b(\beta) = k_b \left(cos\beta + 1\right) \qquad w_s(\alpha) = \frac{1}{2}k_s\alpha^c \tag{1}$$

where $M(\alpha) = \partial w_s(\alpha)/\partial \alpha$. The geometrical significance of β and $\gamma = \pi/2 - \alpha$ is illustrated in Fig. 2b and c. Moreover, k_a, k_b, and k_s represent the extensional, bending, and torsional stiffness, respectively. Symbols $\ell_0 = \left\| \overrightarrow{P_i P_{i+1}} \right\|$, $\ell = \left\| \overrightarrow{p_i p_{i+1}} \right\|$ denote the lengths of the beams in the initial and actual configurations, $\|\cdot\|$ represents the Euclidean norm. It has been observed in [30] that shear energy w_s in Eq. (1) is unsuitable for describing the pronounced change in the concavity of the force-elongation curve of metallic pantographic sheets during a bias elongation test (see Fig. 1). Moreover, the second derivative of the specific energy function w_s, defined in Eq.(1), tends to infinity for $c < 2$ and as α approaches 0, leading to numerical difficulties. Numerical simulations reveal that altering the functions describing axial and bending energies, w_a and w_b, has a negligible impact on the agreement between theoretical and experimental force-elongation curves obtained from a bias elongation test when a large change of concavity of the curve occurs. An alternative phenomenological two-parameter shear energy has been proposed in [30]. This new shear energy is defined by

$$w_s(\alpha) = k_s \left(\alpha \arctan\left(a\alpha\right) - \frac{\log\left(a^2\alpha^2 + 1\right)}{2a} \right) \tag{2}$$

and leads to the simple constitutive law $\alpha \mapsto M(\alpha)$ for the interconnecting hinges defined by

$$M(\alpha) = \frac{\partial w_s(\alpha)}{\partial \alpha} = k_s \arctan\left(a\,\alpha\right), \tag{3}$$

in which k_s and a are the two parameters of the constitutive law. This formulation provides a suitable representation for the force-elongation curve during a bias elongation test, accounting for high changes in concavity, with a single parameter a responsible for the concavity change. Using experimental results (see [30]), the following values of k_s and a have been identified:

- Polyamide pantographic sheet: $a = 5$ and $k_s = 1.66$ N mm (with hinge radius $R = 4.5$ mm),
- Metallic pantographic sheet: $a = 25$ and $k_s = 8.84$ N mm (with hinge radius $R = 5$ mm).

The associated graphs $\alpha \mapsto M(\alpha)$ are presented in Fig. 3. Although this mesoscale model allows for the identification of the bias extension test of polyamide and metallic pantographic sheets, the issue of the microscopic origin of the mesoscale behavior leading to change of concavity on the macroscale remains an open problem. Coming back to Fig. 1, in which two successive loadings are applied, it is evident that a permanent displacement occurs after the first unloading, suggesting the occurrence of plasticity within the hinges. In this work, we aim to shift from the mesoscale to the microscale.

As a 3D structure, the pantographic structure comprises an arrangement of 3D beams interconnected by 3D cylinders (hinges). It has already been observed in the literature that the macroscopic behavior of pantographic sheets depends mainly on their microstructure [35]. The length scale of the microscopic scale is about one
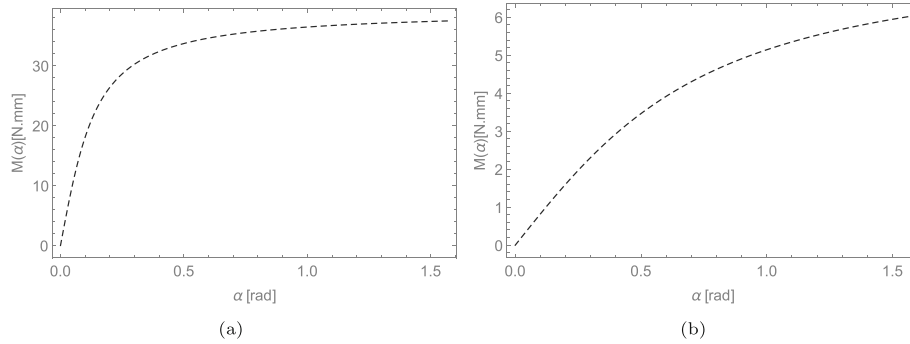
Fig. 3 Graph of $\alpha \mapsto M(\alpha)$ for **a** metallic and **b** polyamide pantographic sheets considering arctan laws obtained by assuming **a** $a = 25$ and $k_s = 8.84$ N mm and **b** $a = 5$ and $k_s = 1.66$ N mm

hundredth of the smallest dimensions of hinges and beams, i.e. of the order of magnitude of 0.1 mm for the pantographic sheets considered in this paper. At this microscale, the constitutive law governing the 3D material behavior of the hinges will be represented in the present work as a 3D elastoplastic Cauchy medium. The mesoscale constitutive law $\alpha \mapsto M(\alpha)$ will be derived as an analytical closed-form solution from the law $(\alpha, r) \mapsto \tau(\alpha, r)$ obtained by solving the 3D problem of a cylinder subjected to pure torsion made of an elastoplastic material.

3 Mesoscopic constitutive equations via micro-meso analysis

This section is devoted to deriving an analytical relationship between torque M and twist angle α for a cylindrical hinge. To do so, we will model the hinge as a cylinder of radius R and height h, while considering the following boundary conditions expressed in cylindrical coordinates:

$$
\begin{cases}
\text{at } z = 0 \; : \quad \underline{u} \cdot \underline{e}_r = 0 \quad \underline{u} \cdot \underline{e}_\theta = 0 \quad (\underset{\sim}{\sigma} \cdot \underline{n}) \cdot \underline{z} = 0 \\
\text{at } z = h \; : \quad \underline{u} \cdot \underline{e}_r = 0 \quad \underline{u} \cdot \underline{e}_\theta = \alpha r \quad (\underset{\sim}{\sigma} \cdot \underline{n}) \cdot \underline{z} = 0 \\
\text{at } r = R \; : \quad \underset{\sim}{\sigma} \cdot \underline{n} = \underline{0}
\end{cases}
\tag{4}
$$

3.1 Elastic cylinder

The elasticity problem reads:

$$
\begin{cases}
\underline{\text{div}}\underset{\sim}{\sigma} = \underline{0} \\
\text{boundary conditions (4)} \\
\underset{\sim}{\sigma} = \lambda \, \text{tr}\underset{\sim}{\varepsilon} + 2\mu \, \underset{\sim}{\varepsilon} \\
\underset{\sim}{\varepsilon}(\underline{u}) = \frac{1}{2}\left(\nabla\underline{u} + (\nabla\underline{u})^T\right)
\end{cases}
\tag{5}
$$

Let consider the kinematically admissible displacements field:

$$
\underline{u} = \frac{\alpha r z}{h}\underline{e}_\theta
\tag{6}
$$

The associated strain field reads:

$$
\underset{\sim}{\varepsilon} = \frac{\alpha r}{2h}\underset{\sim}{A} \qquad\qquad \underset{\sim}{A} := \underline{e}_\theta \otimes \underline{e}_z + \underline{e}_z \otimes \underline{e}_\theta
$$

Using the linear elastic constitutive law, the stress field reads:

$$
\underset{\sim}{\sigma} = \frac{\mu \alpha r}{h}\underset{\sim}{A}
\tag{7}
$$

This stress field is statically admissible so we deduce that Eqs. (6) and (7) give the solution of the elastic problem. The mesoscale constitutive law $\alpha \mapsto M(\alpha)$ is obtained by:

$$M(\alpha) = 2\pi \int_0^R \frac{\mu \alpha r}{h} r^2 dr = \frac{\pi R^4 \mu}{2h} \alpha \tag{8}$$

This solution is applicable in the pure elastic regime of the cylinder in torsion.

3.2 Elastoplasticity modeling at micro level

Elastoplasticity constitutive law considered in this paper will be part of generalized standard (isotropic) materials with Von Mises yield criterion and (isotropic or kinematic) hardening under the assumption of proportional monotonic loading [36].

In this specific context, the elastoplastic constitutive law can be integrated into the so-called *Hencky Mises* constitutive law:

$$\underset{\sim}{\varepsilon}^p = \frac{3}{2} \frac{g(\sigma_{eq} - \sigma_Y)}{\sigma_{eq}} \underset{\sim}{\sigma}^D \tag{9}$$

in which $\underset{\sim}{\sigma}^D$ is the deviatoric part of stress, $\underset{\sim}{\varepsilon}^p$ is the plastic strain and

$$g(\sigma_{eq} - \sigma_Y) = \varepsilon_{eq}^p \qquad \sigma_{eq} - \sigma_Y = \mathcal{R}(\varepsilon_{eq}^p) \qquad g \circ \mathcal{R} = Id \tag{10}$$

with

$$\sigma_{eq} = \sqrt{\frac{3}{2} \underset{\sim}{\sigma}^D : \underset{\sim}{\sigma}^D} \qquad \qquad \varepsilon_{eq}^p = \sqrt{\frac{2}{3} \underset{\sim}{\varepsilon}^p : \underset{\sim}{\varepsilon}^p}$$

The choice of plasticity model is thus related to the choice of an hardening law $\sigma_{eq} \mapsto g(\sigma_{eq} - \sigma_Y)$ or $\varepsilon_{eq}^p \mapsto \mathcal{R}(\varepsilon_{eq}^p)$.

3.3 Elastoplastic cylinder

The onset of plasticity is obtained for the angle α_0 and the couple M_0 such that $\sigma_{eq} = \sigma_Y$, which are equal to:

$$\alpha_0 := \frac{1}{\sqrt{3}} \frac{h}{R} \frac{\sigma_Y}{\mu} \qquad \qquad M_0 := \frac{\pi}{2\sqrt{3}} R^3 \sigma_Y \tag{11}$$

Let now suppose that there exists an inner cylinder of radius $R^{(e)}$ in the elastic regime, while the outer part of the cylinder ($R^{(e)} \leq r \leq R$) is in the elastoplastic regime. Let us assume that the solution is of the form:

$$\underline{u} = u_\theta(r)\underline{e}_\theta \qquad \qquad \underset{\sim}{\sigma} = \tau(r)\underset{\sim}{A} \tag{12}$$

As $\underset{\sim}{A} \cdot \underline{e}_r = 0$, the solution in the inner part of the cylinder ($0 \leq r \leq R^{(e)}$) is the same as in the purely elastic case, i.e.:

$$0 \leq r \leq R^{(e)} : \qquad \underline{u} = \frac{\alpha r z}{h} \underline{e}_\theta \qquad \qquad \underset{\sim}{\sigma} = \frac{\mu \alpha r}{h} \underset{\sim}{A}$$

The radius $R^{(e)}$ is obtained assuming continuity of the equivalent stress σ_{eq} which is equal to σ_Y at the boundary between elastic and plastic parts of the cylinder, i.e.:

$$\sqrt{3} \frac{\mu \alpha R^{(e)}}{h} = \sigma_Y \qquad \qquad R^{(e)} = \frac{\alpha_0}{\alpha} R$$

Let us assume that the displacement solution in the inner part of the cylinder is valid in the entire cylinder:

$$0 \leq r \leq R : \qquad \underline{u} = \frac{\alpha r z}{h} \underline{e}_\theta \qquad \qquad \underset{\sim}{\varepsilon} = \frac{\alpha r}{2h} \underset{\sim}{A} \tag{13}$$

The elastic part of the strain is obtained using the linear elastic constitutive law:

$$\underset{\sim}{\varepsilon}^e = \frac{\tau}{2\mu}\underset{\sim}{A} \tag{14}$$

so that the plastic strain is given by:

$$\underset{\sim}{\varepsilon}^p = \underset{\sim}{\varepsilon} - \underset{\sim}{\varepsilon}^e = \frac{1}{2}\left(\frac{\alpha r}{h} - \frac{\tau}{\mu}\right)\underset{\sim}{A} \tag{15}$$

With $\varepsilon_{eq}^p = \frac{1}{\sqrt{3}}\left(\frac{\alpha r}{h} - \frac{\tau}{\mu}\right)$ and $\sigma_{eq} = \sqrt{3}\tau$, Eq. (10) reads then

$$g(\sqrt{3}\tau - \sigma_Y) = \frac{1}{\sqrt{3}}\left(\frac{\alpha r}{h} - \frac{\tau}{\mu}\right) \tag{16}$$

Using the property $2\pi \int_0^R \frac{\mu\alpha r}{h} r^2 dr = \frac{M_0}{\alpha_0}\alpha$, the constitutive law at the mesoscale reads

$$M(\alpha) = \begin{cases} \dfrac{M_0}{\alpha_0}\alpha & \text{for } \alpha \leq \alpha_0 \\ 2\pi \displaystyle\int_0^{\frac{\alpha_0}{\alpha}R} \dfrac{\mu\alpha r}{h} r^2 dr + 2\pi \displaystyle\int_{\frac{\alpha_0}{\alpha}R}^R \tau(\alpha, r) r^2 dr & \text{for } \alpha \geq \alpha_0 \end{cases} \tag{17}$$

in which τ is solution of (16):
$$\frac{\mu\alpha r}{h} - \tau = \sqrt{3}\mu\, g(\sqrt{3}\tau - \sigma_Y) \tag{18}$$

.

4 Mesoscopic constitutive laws obtained by micro-meso analysis

On the microscale, classical hardening laws are:

- Linear (non-saturating) hardening:

$$R(\varepsilon_{eq}^p) = C\varepsilon_{eq}^p \qquad\qquad g(\sigma_{eq} - \sigma_Y) = \frac{\sigma_{eq} - \sigma_Y}{C} \tag{19}$$

- Power law (non-saturating) hardening:

$$R(\varepsilon_{eq}^p) = K\left(\varepsilon_{eq}^p\right)^{\frac{1}{M}} \qquad\qquad g(\sigma_{eq} - \sigma_Y) = \left(\frac{\sigma_{eq} - \sigma_Y}{K}\right)^M \tag{20}$$

- Exponential (saturating) hardening:

$$R(\varepsilon_{eq}^p) = R_\infty\left(1 - \exp(-b\varepsilon_{eq}^p)\right) \qquad g(\sigma_{eq} - \sigma_Y) = -\frac{1}{b}\log\left(1 - \frac{\sigma_{eq} - \sigma_Y}{R_\infty}\right) \tag{21}$$

In the case of *Hencky Mises* law, the plasticity model can also be defined by the direct choice of the function g, even though the inverse function is not analytically available, e.g.

$$g(\sigma_{eq} - \sigma_Y) = \left(\frac{\sigma_{eq} - \sigma_Y}{C}\right) + \left(\frac{\sigma_{eq} - \sigma_Y}{K}\right)^M \tag{22}$$
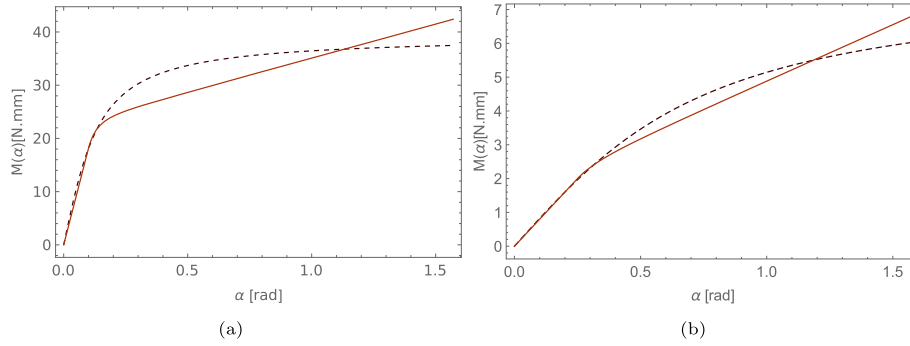
Fig. 4 Graph of $\alpha \mapsto M(\alpha)$ for **a** metallic and **b** polyamide pantographic sheets considering linear hardening (Eq. (24)-solid line) and arctan (Eq. (3)-dashed line) laws. The linear hardening laws are obtained by assuming **a** $\alpha_0 = 0.1$ rad, $M_0 = 18$ N mm, $\chi = 7.59 \times 10^{-2}$, and **b** $\alpha_0 = 0.25$ rad, $M_0 = 2$ N mm, $\chi = 7.14 \times 10^{-1}$. The arctan laws are obtained by assuming **a** $a = 25$ and $k_s = 8.84$ N mm and **b** $a = 5$ and $k_s = 1.66$ N mm

Linear hardening

Introducing $\chi := \frac{C}{3\mu}$, the solution of Eq. (16), with the choice (19) reads

$$\tau = \frac{2}{\pi} \frac{M_0}{(1 + \chi)R^3} \left(1 + \chi \frac{r}{R} \frac{\alpha}{\alpha_0} \right) \tag{23}$$

so that we obtain:

$$M(\alpha) = \begin{cases} \dfrac{M_0}{\alpha_0}\alpha & \text{for } \alpha \leq \alpha_0 \\[2mm] \dfrac{M_0}{1 + \chi} \left(\dfrac{4}{3} - \dfrac{1}{3}\left(\dfrac{\alpha_0}{\alpha}\right)^3 + \chi\dfrac{\alpha}{\alpha_0} \right) & \text{for } \alpha \geq \alpha_0 \end{cases} \tag{24}$$

The case of Elastic-perfectly plastic micro constitutive law is obtained by setting $\chi = 0$.

In Fig. 4 are presented the arctan laws (see Sect. 2) and the law $\alpha \mapsto M(\alpha)$ of Eq. (24) with fitted parameters α_0, M_0 and χ.

Power law hardening

For the choices (20) or (22), (18) can only be solved analytically for $M = 2, 3, 4$ and Eq. (17) leads then to very cumbersome analytical solutions, so that it is preferable to use the following exponential hardening law instead.

Remark For (20) or (22), the case $M = 1$ corresponds to linear hardening.

Exponential hardening

The solution of (16), with the choice (21), reads:

$$\tau = \frac{R_\infty + \sigma_Y}{\sqrt{3}} - \frac{\sqrt{3}\mu}{b} W\left[\frac{bR_\infty}{3\mu} \exp\left[b\left(\frac{R_\infty + \sigma_Y}{3\mu} - \frac{r\alpha}{\sqrt{3}h} \right) \right] \right] \tag{25}$$

in which the function $W(x)$ is the Lambert W function.

Introducing $\xi := \frac{b}{3\mu}$ and $\zeta := \xi R_\infty$, the previous equation reads:

$$\tau = \frac{2M_0}{\pi R^3} + \frac{1}{\sqrt{3}\xi}\left(\zeta - W\left[\zeta \exp\left[\zeta + \frac{2\sqrt{3}\,\xi M_0}{\pi}\frac{1}{R^3}(1 - \frac{r}{R}\frac{\alpha}{\alpha_0}) \right] \right] \right) \tag{26}$$
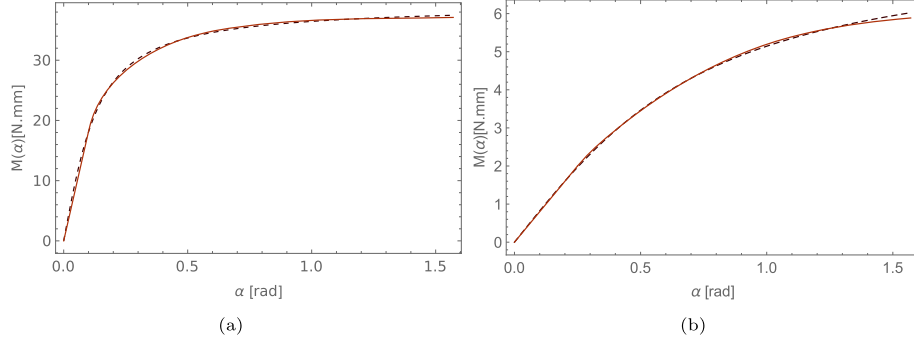
Fig. 5 Graph of $\alpha \mapsto M(\alpha)$ for **a** metallic and **b** polyamid pantographic sheets considering exponential hardening (solid line) and arctan (Eq. (3)-dashed line) laws. The exponential hardening laws are obtained by assuming **a** $\alpha_0 = 0.1$ rad, $M_0 = 18$ N mm, $\xi = 4 \times 10^{-3}$, $\zeta = 0.35$, $R = 0.5$ mm and **b** $\alpha_0 = 0.25$ rad, $M_0 = 2$ N mm, $\xi = 6 \times 10^{-2}$, $\zeta = 1.92$, $R = 0.45$ mm. The arctan laws are obtained by assuming **a** $a = 25$ and $k_s = 8.84$ N mm and **b** $a = 5$ and $k_s = 1.66$ N mm

so that, introducing $\omega[\alpha] = \frac{2\sqrt{3}}{\pi} \frac{M_0 \xi}{R^3} \left(1 - \frac{\alpha}{\alpha_0}\right)$, we obtain for $\alpha \geq \alpha_0$:

$$
\begin{aligned}
M(\alpha) = {}& M_0 \left(\frac{\alpha_0}{\alpha}\right)^3 + \frac{2}{9}(6M_0\xi + \sqrt{3}\pi\zeta R^3)\left(1 - \left(\frac{\alpha_0}{\alpha}\right)^3\right) \\
& - \frac{\pi^2}{18} \frac{R^6}{M_0^3 \xi^4}(6M_0^2\xi^2 + 2\sqrt{3}\pi M_0 R^3 \xi + \pi^2 R^6)\left(\frac{\alpha_0}{\alpha}\right)^3 W\left[\zeta e^\zeta\right] \\
& - \frac{\pi^2}{144} \frac{R^6}{M_0^3 \xi^4}(24M_0^2\xi^2 + 12\sqrt{3}\pi M_0 R^3 \xi + 7\pi^2 R^6)\left(\frac{\alpha_0}{\alpha}\right)^3 \left(W\left[\zeta e^\zeta\right]\right)^2 \\
& - \frac{\pi^3}{648} \frac{R^9}{M_0^3 \xi^4}(12\sqrt{3}M_0\xi + 11\pi R^3)\left(\frac{\alpha_0}{\alpha}\right)^3 \left(W\left[\zeta e^\zeta\right]\right)^3 \\
& - \frac{\pi^4}{432} \frac{R^{12}}{M_0^3 \xi^4}\left(\frac{\alpha_0}{\alpha}\right)^3 \left(W\left[\zeta e^\zeta\right]\right)^4 \\
& + \frac{\pi^2}{18} \frac{R^6}{M_0^3 \xi^4}\left(6M_0^2\xi^2\left(\frac{\alpha_0}{\alpha}\right) + 2\sqrt{3}\pi M_0 R^3 \xi\left(\frac{\alpha_0}{\alpha}\right)^2 + \pi^2 R^6\left(\frac{\alpha_0}{\alpha}\right)^3\right) W\left[\zeta e^{\zeta + \omega[\alpha]}\right] \\
& + \frac{\pi^2}{144} \frac{R^6}{M_0^3 \xi^4}\left(24M_0^2\xi^2\left(\frac{\alpha_0}{\alpha}\right) + 12\sqrt{3}\pi M_0 R^3 \xi\left(\frac{\alpha_0}{\alpha}\right)^2 + 7\pi^2 R^6\left(\frac{\alpha_0}{\alpha}\right)^3\right) \left(W\left[\zeta e^{\zeta + \omega[\alpha]}\right]\right)^2 \\
& + \frac{\pi^3}{648} \frac{R^9}{M_0^3 \xi^4}\left(12\sqrt{3}M_0\xi\left(\frac{\alpha_0}{\alpha}\right)^2 + 11\pi R^3\left(\frac{\alpha_0}{\alpha}\right)^3\right) \left(W\left[\zeta e^{\zeta + \omega[\alpha]}\right]\right)^3 \\
& + \frac{\pi^4}{432} \frac{R^{12}}{M_0^3 \xi^4}\left(\frac{\alpha_0}{\alpha}\right)^3 \left(W\left[\zeta e^{\zeta + \omega[\alpha]}\right]\right)^4
\end{aligned}
\tag{27}
$$

In Fig. 5 are presented the arctan laws (see Sect. 2) and the law $\alpha \mapsto M(\alpha)$ of Eq. (27) with fitted parameters $\alpha_0, M_0, \xi, \zeta$ and R.

5 Phenomenological meso constitutive model inspired by micro-meso modeling

As described in Sect. 2, it was postulated in [30] a 2 parameters heuristic meso modelling of the $M(\alpha)$ constitutive law at meso scale:

$$
M(\alpha) = K \arctan(a\alpha)
\tag{28}
$$

This law, not related to a micro-meso modeling via the elasto-plastic analytical study, did not introduce the definition of a boundary between elastic and plastic regimes. Moreover, for high initial slope, the arctan law is always quickly saturating.

In the previous section, we found, from a complete micro-meso analysis using exponential (or logarithmic) hardening, a precise meso constitutive law capable of reproducing the arctan law and thus a bias test result. Nevertheless, this law is made of 5 parameters and might be too cumbersome for efficient use in an numerical optimization of pantographic structures, e.g. in inverse identification problem.

In this section we propose to introduce a new phenomenological meso-model constitutive law $\alpha \mapsto M(\alpha)$ with a limited number of parameters capable of removing the drawbacks of the arctan law.

To this purpose, we look for a constitutive law $\alpha \mapsto M(\alpha)$ which

- should be made of two parts, one in a (linear) elastic regime, the second in a non-linear plastic regime,
- can be saturated or not in the plastic regime,
- has some consistency with an elastoplastic microscopic behavior,
- derive from an explicit elastic potential,
- is continuously differentiable.

Let introduce the following phenomenological mesoscopic constitutive law, with $n > 0$ and $\chi > 0$:

$$
M(\alpha) = \begin{cases} \dfrac{M_0}{\alpha_0}\alpha & \text{for } \alpha \leq \alpha_0 \\ \dfrac{M_0}{1+\chi}\left(\dfrac{n+1}{n} - \dfrac{1}{n}\left(\dfrac{\alpha_0}{\alpha}\right)^n + \chi\dfrac{\alpha}{\alpha_0}\right) & \text{for } \alpha \geq \alpha_0 \end{cases} \tag{29}
$$

This law:

- is saturating for $\chi = 0$, and non-saturating for $\chi > 0$,
- is consistent with the meso constitutive law analytically obtained with linear hardening for $n = 3$,
- derives from the potential

$$
n \neq 1 \qquad w_s(\alpha) = \begin{cases} \dfrac{1}{2}\dfrac{M_0}{\alpha_0}\alpha^2 & \text{for } \alpha \leq \alpha_0 \\ \dfrac{M_0\alpha}{1+\chi}\left(\dfrac{n+1}{n} + \dfrac{1}{n(n-1)}\left(\dfrac{\alpha_0}{\alpha}\right)^n + \dfrac{\chi}{2}\dfrac{\alpha}{\alpha_0}\right) + C_0 & \text{for } \alpha \geq \alpha_0 \end{cases}
$$

$$
n = 1 \qquad w_s(\alpha) = \begin{cases} \dfrac{1}{2}\dfrac{M_0}{\alpha_0}\alpha^2 & \text{for } \alpha \leq \alpha_0 \\ \dfrac{M_0}{1+\chi}\left(2 + \dfrac{\chi}{2}\dfrac{\alpha}{\alpha_0} - \dfrac{\alpha_0}{\alpha}\log(\alpha)\right) + C_1 & \text{for } \alpha \geq \alpha_0 \end{cases}
$$

in which $C_0 = \dfrac{M_0\alpha_0}{2}\left(1 - \dfrac{2n + \chi(n-1)}{(1+\chi)(n-1)}\right)$ and $C_1 = \dfrac{M_0\alpha_0}{2}\left(1 - \dfrac{4 + \chi - 2\log(\alpha_0))}{\alpha_0(1+\chi)}\right)$,

- is continuously differentiable with

$$
M(\alpha_0) = M_0 \qquad\qquad \left.\dfrac{\partial M}{\partial \alpha}\right|_{\alpha=\alpha_0} = \dfrac{M_0}{\alpha_0}
$$

This law introduces 4 parameters with the following physical meaning:

- M_0 is the couple at the end of linear elastic regime,
- α_0 is the angle at the end of linear elastic regime,
- $\dfrac{\chi}{1+\chi}$ is, for nonsaturating law, the ratio of slope of the asymptotic line in the plastic regime to elastic slope $\dfrac{M_0}{\alpha_0}$,
- $\dfrac{n+1}{n}$ is, for saturating law, the ratio of maximal couple to M_0.

In Fig. 6 are presented the arctan laws (see Sect. 2) and the law $\alpha \mapsto M(\alpha)$ of Eq. (29) with fitted parameters α_0, M_0, χ, n.
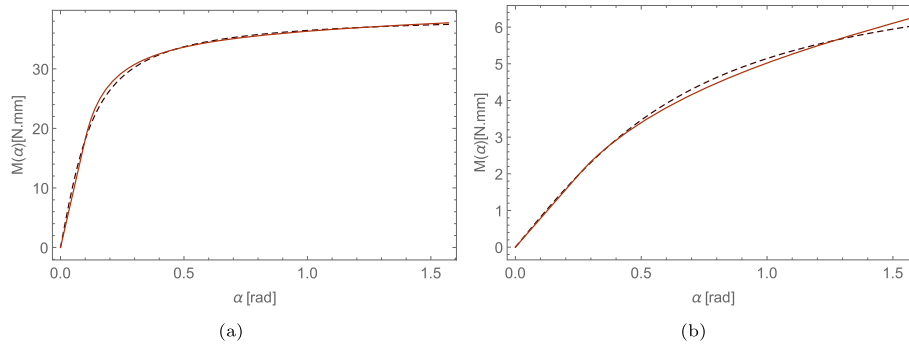
Fig. 6 Graph of $\alpha \mapsto M(\alpha)$ for **a** metallic and **b** polyamid pantographic sheets considering power n (Eq. (29))-solid line) and arctan ((3)-dashed line) laws. The power n laws are obtained by assuming (a) $\alpha_0 = 0.1$ rad, $M_0 = 18$ N mm, $\chi = 6 \times 10^{-3}$, and n = 0.9, and **b** $\alpha_0 = 0.25$ rad, $M_0 = 2$ N mm, $\chi = 0.1$, and n = 10^{-2}. The arctan laws are obtained by assuming **a** $a = 25$ and $k_s = 8.84$ N mm and **b** $a = 5$ and $k_s = 1.66$ N mm

6 Conclusions

Generalized continua are the mathematical models used for precisely describing the exotic mechanical behavior demanded to novel metamaterials [37,38]. The standard continuum mechanics usually associated to the name of Cauchy, albeit very predictive of the behavior of many materials, cannot cover the whole range of possible mechanical behavior. One is obliged to use the the principle of virtual work when she needs to introduce continua models more general than Cauchy's as the postulation scheme based on balance laws cannot be easily extended.

Once the desired generalized continuum model is chosen, then the problem of synthesizing a micro structure governed by chosen generalized continuum arises. In [9,10], it is proven that in the synthesis problem pantographic microstructures play a very relevant role.

The motivation of the analysis presented in this paper was twofold: (1) Understanding and describing the mechanical phenomena occurring in the most important part of pantographic structure, e.g. deformable hinges [39,40]. (2) Giving theoretical indications for designing and constructing pantographic metamaterials showing the largest possible elastic regime [25,41–43].

Concerning point (1), we have obtained strong indications that the force displacement relationship observed in extension bias elongation test is determined not only by elastic phenomena but also by plasticity occurring in the hinge. We remark that we are aware of the limitations of the elastic plastic models at micro level we have introduced. Clearly more sophisticated description of plastic phenomena are possible and desirable. However we believe that at least for polyamide and metallic materials used, our description is satisfactory enough. We found at mesolevel a closed form constitutive equation for torsional moment in function of shear angle in the particular cases of linear or logarithmic hardening. For linear hardening, the mesoconstitutive equation is satisfactory at least qualitatively while for logarithmic hardening, a perfect match with the arctan law proves that the bias extension test can be identified with this particular elasto-plastic law on the micro level. Moreover, the available micro-meso identifications with linear hardening allowed us to conjecture a simple phenomenological relationship between couple and twist angle for pantographic hinges involving only 4 constitutive parameters which is suitable for deducing macro behavior, i.e. Force elongation curve in bias extension test and overall deformed shape of the pantographic structure.

Concerning point (2), we remark that it was a lucky choice to use polyamide in the first bias elongation test for pantographic structures while the choice the metals to be used in 3D printing was less happy: the onset of irreversible plastic deformation is $\alpha_0 = 14°$ for polyamide and $\alpha_0 = 5°$ for metallic pantographs. Moreover, the onset of irreversible plastic deformation occurring for the angle $\alpha_0 = \frac{1}{\sqrt{3}} \frac{h}{R} \frac{\sigma_Y}{\mu}$, better materials with respect to late occurrence of plasticity for a given geometrical configuration are those with greater ratio $\frac{\sigma_Y}{\mu}$.

The performed analysis indicates that some new building strategies and solutions may be required for realizing perfect pivots and elastic hinges: the first proposed use of full cylinder being deformed in torsion seems not completely efficient, albeit it can be exploited for the already used micro materials [22,39,44–46].

Finally, presented results will allow for the design of a novel experimental setup aimed at investigating the micro mechanical properties determining meso saturation effects of couple angle dependence, and change of

concavity in macro force displacement dependence. In particular it seems very promising to use polymeric foam for building pantographic microstructures: their elongation and elastic performances could be outstanding.

Declarations

Author contributions The authors contributed equally to the writing and reviewing of the manuscript.

Data availability No datasets were generated or analysed during the current study.

Competing interests The authors declare no competing interests.

References

1. Barchiesi, E., dell'Isola, F., Laudato, M., Placidi, L., Seppecher, P.: A 1D continuum model for beams with pantographic microstructure: asymptotic micro-macro identification and numerical results. In: dell'Isola, F., Eremeyev, V.A., Porubov, A. (eds.) Advances in Mechanics of Microstructured Media and Structures. Springer, Berlin (2018)
2. Barchiesi, E., dell'Isola, F., Seppecher, P., Turco, E.: A beam model for duoskelion structures derived by asymptotic homogenization and its application to axial loading problems. Eur. J. Mech. A Solids **27**, 104848 (2023)
3. Barchiesi, E., Spagnuolo, M., Placidi, L.: Mechanical metamaterials: a state of the art. Math. Mech. Solids **24**(1), 212–234 (2019)
4. Barchiesi, E., dell'Isola, F., Hild, F.: On the validation of homogenized modeling for bi-pantographic metamaterials via digital image correlation. Int. J. Solids Struct. **208–209**, 49–62 (2021)
5. Auffray, N., dell'Isola, F., Eremeyev, V.A., Madeo, A., Rosi, G.: Analytical continuum mechanics à la Hamilton–Piola least action principle for second gradient continua and capillary fluids. Math. Mech. Solids **20**(4), 375–417 (2015)
6. Ciallella, A.: Research perspective on multiphysics and multiscale materials: a paradigmatic case. Contin. Mech. Thermodyn. **32**(3), 527–539 (2020)
7. dell'Isola, F., Andreaus, U., Placidi, L.: At the origins and in the vanguard of peridynamics, non-local and higher-gradient continuum mechanics: an underestimated and still topical contribution of Gabrio Piola. Math. Mech. Solids **20**(8), 887–928 (2015)
8. dell'Isola, F., Corte, A.D., Giorgio, I.: Higher-gradient continua: the legacy of Piola, Mindlin, Sedov and Toupin and some future research perspectives. Math. Mech. Solids **22**(4), 852–872 (2015)
9. dell'Isola, F., Seppecher, P., Spagnuolo, M., et al.: Advances in pantographic structures: design, manufacturing, models, experiments and image analyses. Contin. Mech. Thermodyn. **31**(4), 1231–1282 (2019)
10. dell'Isola, F., Seppecher, P., Alibert, J.J., Lekszycki, T., Grygoruk, R., Pawlikowski, M., Steigmann, D., Giorgio, I., Andreaus, U., Turco, E., Gołaszewski, M., et al.: Pantographic metamaterials: an example of mathematically driven design and of its technological challenges. Contin. Mech. Thermodyn. **31**(4), 851–884 (2019)
11. Turco, E., Misra, A., Pawlikowski, M., dell'Isola, F., Hild, F.: Enhanced Piola–Hencky discrete models for pantographic sheets with pivots without deformation energy: numerics and experiments. Int. J. Solids Struct. **147**, 94–109 (2018). https://doi.org/10.1016/j.ijsolstr.2018.05.015
12. Turco, E., dell'Isola, F., Cazzani, A., Rizzi, N.L.: Hencky-type discrete model for pantographic structures: numerical comparison with second gradient continuum models. Z. Angew. Math. Phys. **67**(4), 85–128 (2016). https://doi.org/10.1007/s00033-016-0681-8
13. Scerrato, D., Zhurba Eremeeva, I.A., Lekszycki, T., et al.: On the effect of shear stiffness on the plane deformation of linear second gradient pantographic sheets. Z. Angew. Math. Mech. **96**(11), 1268–1279 (2016). https://doi.org/10.1002/zamm.201600066
14. Turco, E., Misra, A., Sarikaya, R., Lekszycki, T.: Quantitative analysis of deformation mechanisms in pantographic substructures: experiments and modeling. Contin. Mech. Thermodyn. **31**(1), 209–223 (2019). https://doi.org/10.1007/s00161-018-0678-y
15. Gutmann, F., Stilz, M., Patil, S., Fischer, F., Hoschke, K., Ganzenmüller, G., Hiermaier, S.: Miniaturization of non-assembly metallic pin-joints by LPBF-based additive manufacturing as perfect pivots for pantographic metamaterials. Materials **16**(5), 1797 (2023). https://doi.org/10.3390/ma16051797
16. Golaszewski, M., Grygoruk, R., Giorgio, I., Laudato, M., Cosmo, F.D.: Metamaterials with relative displacements in their microstructure: technological challenges in 3d printing, experiments and numerical predictions. Contin. Mech. Thermodyn. **31**(4), 1015–1034 (2018). https://doi.org/10.1007/s00161-018-0692-0
17. Turco, E., Gołaszewski, M., Giorgio, I., Placidi, L.: Can a Hencky-type model predict the mechanical behaviour of pantographic lattices? Math. Model. Solid Mech. **69**, 285–311 (2017). https://doi.org/10.1007/978-981-10-3764-1_18
18. Yang, H., Ganzosch, G., Giorgio, I., Abali, B.E.: Material characterization and computations of a polymeric metamaterial with a pantographic substructure. Z. Angew. Math. Phys. **69**(4), 105–116 (2018)
19. Turco, E., Barcz, K., Pawlikowski, M., Rizzi, N.L.: Non-standard coupled extensional and bending bias tests for planar pantographic lattices. Part I: numerical simulations. Z. Angew. Math. Phys. **67**(5), 122–116 (2016)
20. Turco, E., Rizzi, N.L.: Pantographic structures presenting statistically distributed defects: numerical investigations of the effects on deformation fields. Mech. Res. Commun. **77**, 65–69 (2016). https://doi.org/10.1016/j.mechrescom.2016.09.006

21. Spagnuolo, M., Peyre, P., Dupuy, C.: Phenomenological aspects of quasi-perfect pivots in metallic pantographic structures. Mech. Res. Commun. **101**, 103415–16 (2019). https://doi.org/10.1016/j.mechrescom.2019.103415
22. Desmorat, B., Spagnuolo, M., Turco, E.: Stiffness optimization in nonlinear pantographic structures. Math. Mech. Solids **25**(12), 2252–2262 (2020). https://doi.org/10.1177/1081286520935503
23. Giorgio, I., Ciallella, A., Scerrato, D.: A study about the impact of the topological arrangement of fibers on fiber-reinforced composites: some guidelines aiming at the development of new ultra-stiff and ultra-soft metamaterials. Int. J. Solids Struct. **203**, 73–83 (2020)
24. Placidi, L., Andreaus, U., Giorgio, I.: Identification of two-dimensional pantographic structure via a linear D4 orthotropic second gradient elastic model. J. Eng. Math. **103**(1), 1–21 (2017). https://doi.org/10.1007/s10665-016-9856-8
25. De Angelo, M., Spagnuolo, M., D'Annibale, F., et al.: The macroscopic behavior of pantographic sheets depends mainly on their microstructure: experimental evidence and qualitative analysis of damage in metallic specimens. Contin. Mech. Thermodyn. **31**(4), 1181–1203 (2019). https://doi.org/10.1007/s00161-019-00757-3
26. Giorgio, I.: Numerical identification procedure between a micro-Cauchy model and a macro-second gradient model for planar pantographic structures. Z. Angew. Math. Phys. **67**(4), 95–117 (2016). https://doi.org/10.1007/s00033-016-0692-5
27. Spagnuolo, M., Yildizdag, M.E., Andreaus, U., Cazzani, A.: Are higher-gradient models also capable of predicting mechanical behavior in the case of wide-knit pantographic structures? Math. Mech. Solids **26**(1), 18–29 (2021)
28. Spagnuolo, M., Reccia, E., Ciallella, A., Cazzani, A.: Matrix-embedded metamaterials: applications for the architectural heritage. Math. Mech. Solids **27**(10), 2275–2286 (2022)
29. dell'Isola, F., Giorgio, I., Pawlikowski, M., Rizzi, N.L.: Large deformations of planar extensible beams and pantographic lattices: heuristic homogenization, experimental and numerical examples of equilibrium. Proc. R. Soc. A Math. Phys. Eng. Sci. **472**(2185), 20150790 (2016)
30. Valle, G.L., Spagnuolo, M., Turco, E., Desmorat, B.: A new torsional energy for pantographic sheets. Z. Angew. Math. Phys. **74**(2), 67 (2023)
31. Yildizdag, M.E., Ciallella, A., D'Ovidio, G.: Investigating wave transmission and reflection phenomena in pantographic lattices using a second-gradient continuum model. Math. Mech. Solids **28**(8), 1776–1789 (2023)
32. Turco, E., Barcz, K., Pawlikowski, M., Rizzi, N.L.: Non-standard coupled extensional and bending bias tests for planar pantographic lattices. Part I: numerical simulations. Z. Angew. Math. Phys. **67**, 1–16 (2016)
33. Turco, E., Gołaszewski, M., Cazzani, A., Rizzi, N.L.: Large deformations induced in planar pantographic sheets by loads applied on fibers: experimental validation of a discrete lagrangian model. Mech. Res. Commun. **76**, 51–56 (2016). https://doi.org/10.1016/j.mechrescom.2016.07.001
34. Turco, E., Misra, A., Pawlikowski, M., dell'Isola, F., Hild, F.: Enhanced Piola–Hencky discrete models for pantographic sheets with pivots without deformation energy: numerics and experiments. Int. J. Solids Struct. **147**, 94–109 (2018). https://doi.org/10.1016/j.ijsolstr.2018.05.015
35. De Angelo, M., Spagnuolo, M., D'annibale, F., Pfaff, A., Hoschke, K., Misra, A., Dupuy, C., Peyre, P., Dirrenberger, J., Pawlikowski, M.: The macroscopic behavior of pantographic sheets depends mainly on their microstructure: experimental evidence and qualitative analysis of damage in metallic specimens. Contin. Mech. Thermodyn. **31**, 1181–1203 (2019)
36. Lemaitre, J., Chaboche, J.L., Benallal, A., Desmorat, R.: Mécanique des Matériaux Solides - 3ème édition. Physique. Dunod (2009)
37. Greco, F., Leonetti, L., Lonetti, P., Luciano, R., Pranno, A.: A multiscale analysis of instability-induced failure mechanisms in fiber-reinforced composite structures via alternative modeling approaches. Compos. Struct. **251**, 112529 (2020)
38. De Maio, U., Greco, F., Leonetti, L., Luciano, R., Nevone Blasi, P., Vantadori, S.: A refined diffuse cohesive approach for the failure analysis in quasibrittle materials—part II: application to plain and reinforced concrete structures. Fatigue Fract. Eng. Mater. Struct. **42**(12), 2764–2781 (2019)
39. Ciallella, A., Pasquali, D., Gołaszewski, M., D'Annibale, F., Giorgio, I.: A rate-independent internal friction to describe the hysteretic behavior of pantographic structures under cyclic loads. Mech. Res. Commun. **116**, 103761–15 (2021)
40. Stilz, M., Plappert, D., Gutmann, F., Hiermaier, S.: A 3D extension of pantographic geometries to obtain metamaterial with semi-auxetic properties. Math. Mech. Solids **27**(4), 673–686 (2022)
41. Ciallella, A., Steigmann, D.J.: Unusual deformation patterns in a second-gradient cylindrical lattice shell: numerical experiments. Math. Mech. Solids (2022). https://doi.org/10.1177/10812865221101820
42. Alibert, J.-J., Seppecher, P., dell'Isola, F.: Truss modular beams with deformation energy depending on higher displacement gradients. Math. Mech. Solids **8**(1), 51–73 (2003)
43. La Valle, G., Ciallella, A., Falsone, G.: The effect of local random defects on the response of pantographic sheets. Math. Mech. Solids **27**(10), 2147–2169 (2022). https://doi.org/10.1177/10812865221103482
44. Spagnuolo, M., Barcz, K., Pfaff, A., Franciosi, P., dell'Isola, F.: Qualitative pivot damage analysis in aluminum printed pantographic sheets: numerics and experiments. Mech. Res. Commun. **83**, 47–52 (2017)
45. Spagnuolo, M., Yildizdag, M.E., Pinelli, X., Cazzani, A., Hild, F.: Out-of-plane deformation reduction via inelastic hinges in fibrous metamaterials and simplified damage approach. Math. Mech. Solids **27**(6), 1011–1031 (2022)
46. Abali, B.E., Yang, H., Papadopoulos, P.: A computational approach for determination of parameters in generalized mechanics. In: Altenbach, H., Müller, W., Abali, B. (eds.) Higher Gradient Materials and Related Generalized Continua, pp. 1–18. Springer, Berlin (2019)